

**LA-UR-23-30247**

Accepted Manuscript

## **Simulating gas-filled neutron detector responses with DRIFT**

Mullen, Austin Daniel  
Andrews, Madison Theresa  
Rondini, Lucia Isabella  
Thompson, Cole Joseph

Provided by the author(s) and the Los Alamos National Laboratory (2024-02-23).

**To be published in:** Nuclear Instruments and Methods in Physics Research Section A: Accelerators, Spectrometers, Detectors and Associated Equipment

**DOI to publisher's version:** 10.1016/j.nima.2024.169164

**Permalink to record:**

<https://permalink.lanl.gov/object/view?what=info:lanl-repo/lareport/LA-UR-23-30247>



Los Alamos National Laboratory, an affirmative action/equal opportunity employer, is operated by Triad National Security, LLC for the National Nuclear Security Administration of U.S. Department of Energy under contract 89233218CNA000001. By approving this article, the publisher recognizes that the U.S. Government retains nonexclusive, royalty-free license to publish or reproduce the published form of this contribution, or to allow others to do so, for U.S. Government purposes. Los Alamos National Laboratory requests that the publisher identify this article as work performed under the auspices of the U.S. Department of Energy. Los Alamos National Laboratory strongly supports academic freedom and a researcher's right to publish; as an institution, however, the Laboratory does not endorse the viewpoint of a publication or guarantee its technical correctness.

# 1 Simulating Gas-Filled Neutron Detector Responses with DRiFT

2 A.D. Mullen<sup>\*1</sup>, M.T. Andrews<sup>1</sup>, L.I. Rondini<sup>1</sup>, C.J. Thompson<sup>1</sup>

3 1. XTD-RTA: Radiation Transport Applications, Los Alamos National Laboratory, P.O. Box 1663, Los Alamos, 87544,  
4 New Mexico, United States

5 \*Corresponding author, [austin.mullen@lanl.gov](mailto:austin.mullen@lanl.gov)

6 **Abstract** – Gas-filled neutron detectors have numerous applications across the nuclear engineering  
7 and nuclear physics fields. The ability to accurately model and simulate these detectors is  
8 important for those applications but is currently limited by the lack of readily-usable detector  
9 response software. Recently, the capabilities of DRiFT, a Detector Response Function Toolkit, were  
10 expanded to model gas-filled, He-3 and BF<sub>3</sub>, neutron detectors so that, combined with the radiation  
11 transport capabilities of the MCNP code, a high-fidelity treatment of gas-filled neutron detectors can  
12 be obtained. This model has been validated by an experiment carried out with the Epithermal  
13 Neutron Multiplicity Counter and its capabilities have been demonstrated in two additional  
14 experiments. This work shows that utilizing DRiFT to post-process MCNP outputs produces more  
15 accurate results than using the MCNP code alone, reducing the difference between experimental  
16 and simulated results for measurements taken near the end of a He-3 tube, where the MCNP code  
17 struggles to model inactive regions of the detector, from a maximum of 35% with the MCNP code  
18 alone to 15% with the MCNP code plus DRiFT. DRiFT's diagnostic capabilities are also  
19 demonstrated with measurements for scenarios when pulse pileup or room return effects are  
20 significant and must be considered. Altogether, these measurements underpin the ability of DRiFT  
21 to accurately model and predict the behavior of gas-filled neutron detectors, making it a valuable  
22 tool for the design and testing of systems and experiments that utilize these detectors.

## 23 Introduction

24 The simulation and modeling of gas-filled neutron detectors has important applications  
25 across a variety of fields, including in nuclear safeguards [1], nuclear security [2], and nuclear  
26 physics applications [3]. The MCNP, or Monte Carlo N-Particle [4], code is extremely powerful for  
27 simulating the transport of neutrons to, and interactions within, a detector, but has relatively limited  
28 ability to simulate the response of that detector to incident radiation. DRiFT, a Detector Response  
29 Function Toolkit, is a pre-compiled executable software toolkit developed in C++, and was  
30 designed to complement the radiation transport capabilities of the MCNP code with a detailed  
31 simulation of a detector's response [5]. The capabilities of DRiFT have previously been  
32 demonstrated for scintillator detectors and related electronics [6,7,8], and further developments  
33 of the code are planned to support semiconductor detectors [9]. This work focuses on the new  
34 capability of DRiFT to post-process MCNP outputs to model gas-filled detector responses to  
35 neutron irradiation, which has recently been publicly released [10].

36 Gas-filled neutron detectors, particularly those filled with He-3, serve an important role in  
37 nuclear experimentation due to their suitability for thermal neutron measurements. First, He-3  
38 and BF<sub>3</sub>, another popular gas fill, have naturally high thermal neutron cross sections, maximizing  
39 interaction rates within the detector [11]. Second, gas-filled neutron detectors are largely  
40 insensitive to gamma radiation, when compared to their sensitivity to neutrons, making them ideal  
41 for use in a mixed radiation field like a spent fuel pool where only neutron interactions are of  
42 interest. Finally, gas-filled detectors are very reliable and resilient in high radiation fluxes. Gas-  
43 filled neutron detectors are often used in conjunction with a moderator such as polyethylene, as  
44 they are relatively insensitive to fast neutrons given the orders of magnitude smaller capture cross  
45 section in this energy region. Multiple gas-filled detectors are commonly used together in neutron

46 well counters, which takes advantage of the detection efficiency provided by the large thermal  
47 neutron cross sections intrinsic to gas-filled detectors [12].

48 The MCNP code is an extensively well-validated and powerful Monte Carlo radiation  
49 transport code. The MCNP code has some capability to model gas tube physics; these include  
50 the ability to simulate effects of tube pressure on detection efficiency and the wall effects if protons  
51 and tritons are explicitly simulated. More nuanced effects on gas-filled detector response are  
52 missed, however. In many gas tubes, the ends of the tube are rendered inactive to remove  
53 nonlinear end-tube effects due to distortions in the electric fields in these regions. The MCNP  
54 code does not model this effect, so users must completely neglect neutron interactions in the  
55 inactive zones, even when these interactions could result in energy deposition in the active region  
56 of the detector. Additionally, interactions in the inactive regions of the detector may contribute to  
57 the detector signal, as charge created in these regions can still be collected but is generally not  
58 multiplied [13]; the MCNP code does not model this effect either. Finally, the MCNP code does  
59 not model downstream electronic effects from the preamplifier, pulse pileup, or detector dead  
60 time, which may degrade the accuracy of its results in some situations. More accurate modeling  
61 of gas-filled detectors can be performed using a combination of Geant4 and Garfield++, and is  
62 likely possible using the MCNP code and Garfield ++, but this requires extensive user modification  
63 and expertise in these software to perform [14,15]. DRiFT is intended to complement the  
64 capabilities of the MCNP code by modeling these effects and providing the user a human-  
65 readable event-by-event readout including details for every event that occurs in the detector.

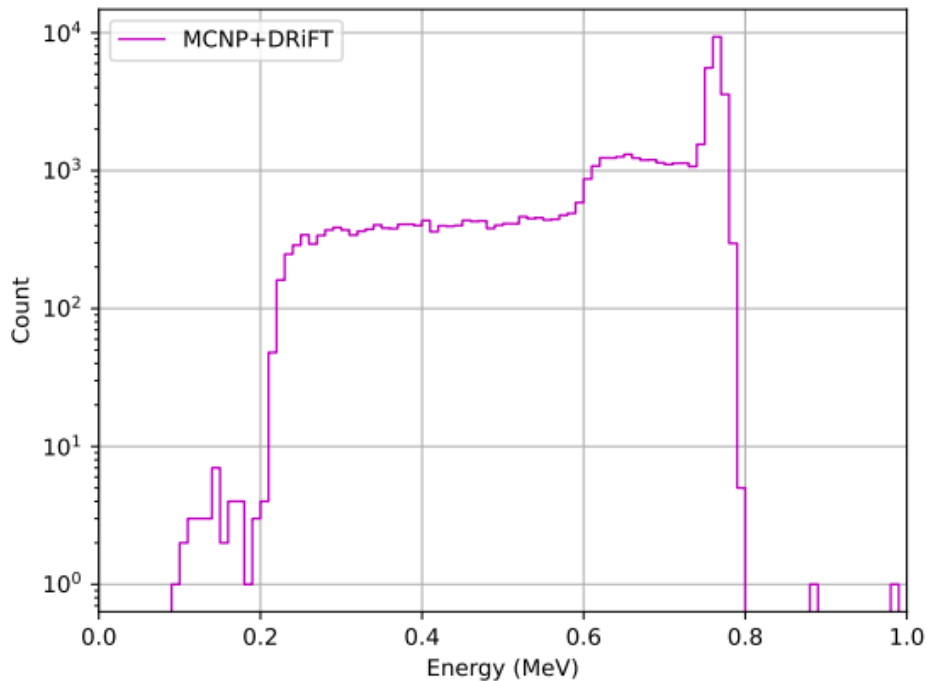
## 66 Gas Detector Physics in DRiFT

67 The principles of operation of a gas-filled neutron detector are outlined in this section using  
68 a He-3 tube as an example; the general mechanisms at play are the same regardless of the  
69 choice of fill gas [16]; the types of charged ions generated and the energy deposited will change  
70 with different fill gasses. First, a thermal neutron interacts in the detector volume via absorption  
71 on a He-3 nucleus. This results in the creation of two charged ions: a proton and a triton. The  
72 proton and triton are created antiparallel and with energies of 0.573 MeV and 0.191 MeV,  
73 respectively. These ions deposit their energy in the gas as they slow, creating electron-ion pairs  
74 along their tracks. It is possible for the proton, triton, or both ions to travel into the wall of the  
75 detector before losing all of their energy. In this case, the energy deposited by that ion in the  
76 detector's wall is not registered by the detector. The electron-ion pairs created by the passage of  
77 the charged particles are then separated by an applied electric field. For a cylindrical detector,  
78 the electrons are directed towards the central anode wire and the positively charged ions are  
79 directed towards the detector's outer wall. Once the electrons reach a sufficiently short distance  
80 from the anode wire, known as the critical radius, the electric field becomes strong enough to  
81 create a multiplicative avalanche, known as the Townsend avalanche, where the acceleration of  
82 the electrons in the intense electric field leads to further ionizations in electron-atom interactions.  
83 The electrons travelling towards the anode create a very fast (less than a nanosecond) signal  
84 pulse, though its magnitude is small due to the short distance travelled by the electrons to the  
85 anode wire, and thus it may not be observable with the detector electronics used. Most of the  
86 electronic signal is generated from the ions created in the avalanche and accelerated away from  
87 the anode wire. After a short time – on the order of one or several microseconds after the start of  
88 the Townsend avalanche – the contribution of ions is ignored by the finite (often around a  
89 microsecond) shaping time of the detector electronics. At this point, the electronics reading the  
90 signal from the tube have returned to their baseline.

91 Each step in the process described above is simulated in DRIFT. To start, a neutron  
92 absorption on the fill gas is read in from the MCNP Particle Track (PTRAC) output. The PTRAC  
93 file provides DRIFT information on where the neutron interacts in the detector, along with an  
94 absolute time stamp for when the interaction occurs. Each individual neutron absorption recorded  
95 in the PTRAC file is treated as its own event in DRIFT. Note that only neutrons need to be  
96 recorded in the PTRAC file, not the charged particles resulting from the absorptions; this allows  
97 the MCNP code to be run using parallelization as of version MCNP6.3. Charged particles are  
98 created at the location of the absorption, and their travel through the gas is modeled. The range  
99 and stopping power of these ions are determined using pre-generated data tables from the  
100 Stopping and Range of Ions in Matter (SRIM) software [17]. This information is then used in  
101 conjunction with data tables generated using Garfield++ [18], a toolkit for the simulation of particle  
102 detectors based on ionization in gases, which interfaces to Magboltz [19]. The data tables, which  
103 are pre-compiled and included with the DRIFT executable, contain information about electron drift  
104 velocities at different electric field strengths, the number of electron-ion pairs generated by  
105 protons and tritons in the gas, and the number of electrons generated in an avalanche. At this  
106 point in the simulation, these data tables are used to calculate the range of the ion's path through  
107 the gas and the number of electron-ion pairs created along the charged particle's track.

108 The drift of the electrons through the gas towards the anode wire is then modeled using  
109 the electron drift velocities provided in the data tables, which depend on the composition and  
110 pressure of the gas in the detector. The timing of the electron's travel is preserved to generate  
111 an accurate pulse shape. Once the electrons reach the critical radius, data tables generated  
112 using Garfield++ are used again to model the multiplication of electrons at the anode, with the  
113 number of electrons generated during the Townsend avalanche stochastically generated for each  
114 primary electron. The final number of electrons generated in the avalanche, along with the timing  
115 information preserved from the electron's path through the gas and the timing of the positively  
116 charged ions created in the avalanche drifting away from the anode wire, is used with the overall  
117 capacitance of the gas-filled tube to calculate the final signal pulse using semi-empirical equations  
118 derived from Wilkinson [20].

119 Several potential effects previously mentioned are also modeled during this process. First,  
120 it is possible for either or both heavy charged particles resulting from the neutron capture in the  
121 gas to have a sufficiently long path length so as to travel into the wall of the detector. In this case,  
122 electron-ion pairs that would have otherwise been created in the gas are instead neglected, and  
123 the total apparent energy deposition in the gas is reduced. This effect can be seen in Figure 1.  
124 Second, it is possible for a neutron to interact in the active region of the detector, but near one of  
125 the inactive end regions. In this case, it is possible for an ion to travel from the point of the neutron  
126 capture into the inactive region; electron-ion pairs that are generated in this inactive region are  
127 collected but not multiplied in an avalanche, and again the apparent energy deposition in the  
128 detector is reduced. The inverse is also true: a neutron may interact in an inactive region of the  
129 detector, and one of the resulting ions may travel into the active region, deposit energy, and be  
130 recorded. In this way, interactions that occur in the inactive region of the detector may still be  
131 registered as detector events, depending on the energy deposition of the ion in the active region  
132 and the minimum charge collection required to pass the detector system's lower-level  
133 discriminator (LLD). This effect can also be seen in the low-energy events in Figure 1.



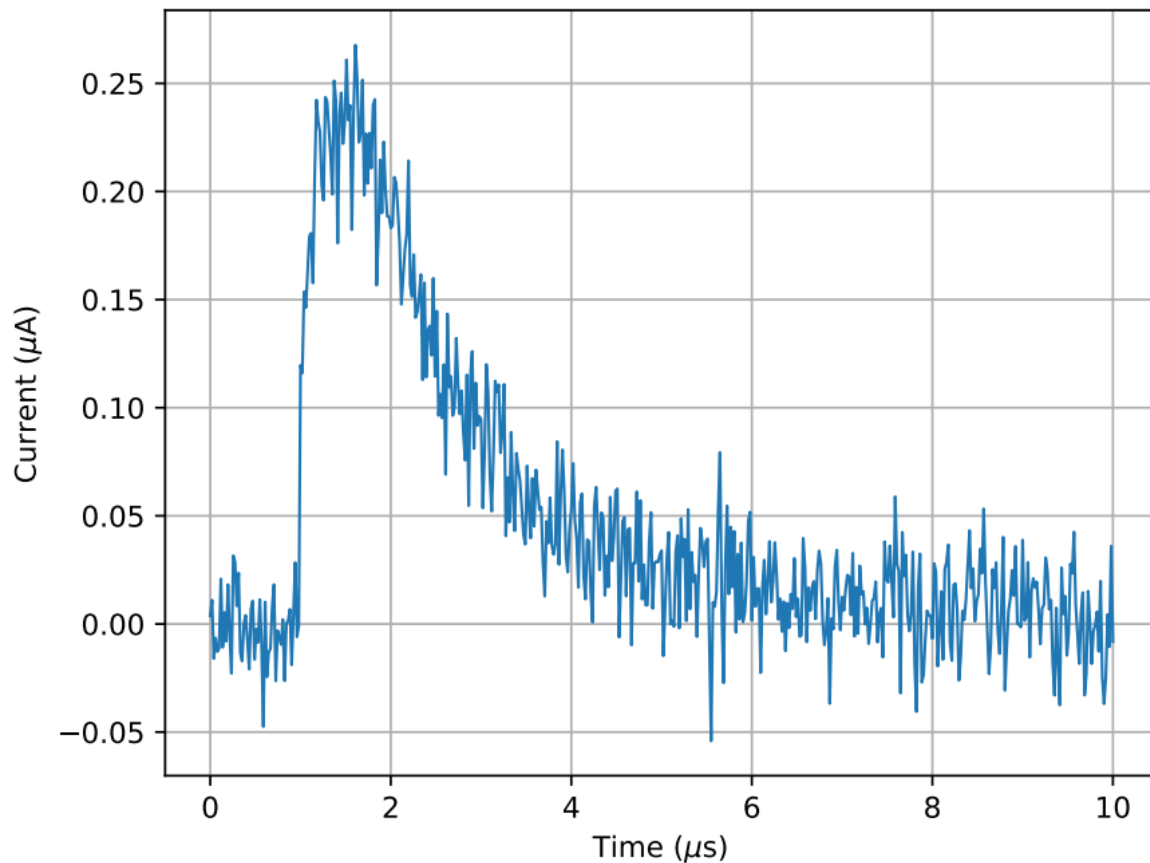
134

135 Figure 1: A sample energy spectrum of a He-3 detector modeled in DRiFT. The effects of  
 136 charged particles travelling into the walls of the detector can be seen in the wall effect  
 137 continuum between around 200 keV to 764 keV. Events that occur below 200 keV are due  
 138 either to both charged particles travelling into the wall of the detector, or one or both charged  
 139 particles depositing energy in the inactive end-tube regions.

140 DRiFT then models the effects of a charge-sensitive preamplifier converting the charge  
 141 collected at the anode to a current pulse. The pulse height and shape are taken from the gas  
 142 tube model described above and converted into a voltage pulse by the simulated preamplifier.  
 143 The shape of the pulse itself is modified according to the shaping time constant of the preamplifier,  
 144 which is provided by the user. Several electronic effects are possible depending on user-specified  
 145 settings. Events that occur close together in time can pileup on each other; that is, there is not  
 146 enough time between events for the electronics to distinguish between them, and they are treated  
 147 as a single event with the total energy deposition being the sum of the two individual events'  
 148 energy depositions. The prevalence of this effect is determined both by the neutron interaction  
 149 rate and the shaping time constant of the preamplifier. Double pulsing is also possible, where  
 150 photons or cations generated in an initial detection event trigger a second, spurious Townsend  
 151 avalanche, and the resulting electronic signal is registered by the preamplifier. This can also be  
 152 modeled by DRiFT, where the probability of spurious double pulsing is determined largely by the  
 153 mix of primary and quench gasses in the detector. It is also possible for a gas tube to experience  
 154 dead time; that is, the tube can be rendered inactive for a time after an event is recorded, as the  
 155 cloud of positively charged ions shrouding the anode wire reduce the electric field in the detector  
 156 sufficiently to prevent new detector events from being recorded until the electric field returns to  
 157 normal strength. This dead time can be either paralyzable or non-paralyzable, where, in a  
 158 paralyzable detector, additional events that occur during the detector's dead time serve to extend  
 159 that dead time even longer. The length of this dead time can be defined by the user in the form  
 160 of a time window, along with whether the dead time should be paralyzable or non-paralyzable.

161 Finally, a user-defined lower-level discriminator (LLD) can be employed to discard events that fail  
162 to record enough energy in the detector. This can be done either directly based on charge  
163 collected by the preamplifier or on the reconstructed energy of the event in the detector,  
164 depending on user preferences.

165 At the end of the simulation, DRiFT outputs an ASCII formatted list of all detection events  
166 that have occurred. The information available in this event-by-event output is configurable by the  
167 user, and can include information on the interaction time, charge collected, reconstructed energy,  
168 and whether the event is correlated to events in other detectors. This correlation can be done  
169 either using the Monte Carlo truth information provided by the MCNP code or a user-specified  
170 coincidence time window. DRiFT can also output diagnostic information, such as the source  
171 neutron's initial energy and whether the event was due to room return or affected by pulse pileup.  
172 Optionally, DRiFT can also output individual pulse shapes for events in the detector for further  
173 analysis, an example of which can be seen in Figure 2.



174  
175 Figure 2: A sample pulse shape for a neutron interaction in a nominal He-3 tube filled to 10  
176 atmospheres with 1800 V applied. The shaping time of the preamplifier was set to be 1  
177 microsecond.

### 178 Specifying Gas Detector Settings in DRiFT

179 A number of parameters are available to customize the behavior of the gas-filled detector  
180 and its associated preamplifier in DRiFT and are outlined in Table 1 and Table 2. Note that these

181 tables are not exhaustive but present the most important and common options available to users.  
 182 More information can be found in the DRiFT user manual, which is included with the public release  
 183 of DRiFT gas-filled detector capabilities.

184 Table 1: The DRiFT parameters available for customization in the Gas module. All parameters  
 185 are defined in the input file as <Keyword>=<Value>.

PARAMETER	DESCRIPTION
call	Always Gas
geometry	The geometry of the gas-filled detector; <i>cylinder</i> by default, with <i>sphere</i> also supported
gas1 and gas2	The fill and quench gas, respectively; <i>He-3</i> and <i>CO<sub>2</sub></i> by default, with <i>BF<sub>3</sub></i> and <i>CH<sub>4</sub></i> also supported
comp1 and comp2	The relative compositions of the fill and quench gases; defaults to 100% fill gas with ranges between 95% and 100% supported
voltage	The applied voltage to the tube; defaults to 1600 V with ranges between 1000 V to 1900 V supported
temperature and temperature_units	The temperature of the tube in the specified units; defaults to 293 K with ranges between 253 K and 293 K supported
pressure	The pressure of the tube, in atmospheres; defaults to 1 atm with ranges between 1 atm and 10 atm supported
tube_length and tube_radius	The length and radius of the tube, in centimeters; defaults to 40.6 cm and 1.25 cm, respectively
wire_radius	The radius of the central anode wire, in centimeters; defaults to 0.0005 cm
tube_base_x/y/z	The location of the gas tube(s) in space, with units of centimeters; the values entered here should be consistent with the location of the detector cells specified in the MCNP input deck
anode_orientation_x/y/z	The orientation of the gas tube(s) in space; defaults to all tubes aligned with the Z axis
inactive_area	Whether to simulate inactive areas at the ends of the gas tube(s); defaults to no inactive area simulations
inactive_bottom, and inactive_top	The size of inactive areas at the ends of the gas tube(s), in centimeters; defaults to 3 cm in both cases

186

187 Table 2: The DRiFT parameters available for customization in the Gas\_Preamplifier module. All  
 188 parameters are defined in the input file as <Keyword>=<Value>.

PARAMETER	DESCRIPTION
call	Always <i>Gas_Preamplifier</i>

pileup	Whether to simulate pulse pileup for events that occur close in time temporally; defaults to no pulse pileup
shaping_time_constant	The shaping time constant determining the electronic pulse die-away time, in seconds; defaults to the load resistance multiplied by the tube capacitance, below. If <code>shaping_time_constant</code> is provided, the values for resistance and capacitance are ignored.
resistance	The load resistance, used to determine the shaping time constant, in ohms. Defaults to 10,000 ohms.
capacitance	The tube capacitance, used to determine the shaping time constant, in farads. Defaults to $10^{-10}$ farads.
dead_time_enable	Whether to simulate dead time in the tube; defaults to no dead time
dead_time	The dead time in the tube, in seconds; defaults to 0 s
paralyzable	Whether the tube's dead time is paralyzable; defaults to not paralyzable
LLD and LLD_units	The lower-level discriminator of the preamplifier, in specified units of energy or charge; defaults to 0 MeV
pulse_offset	The fraction into a digitized trace the simulated pulse should fall; defaults to 0.1, e.g. the start of the pulse (absolute time zero) will be located 10% of the way into the digitizer trace
pulse_shape_bins	The number of bins to use when recording an electronic pulse; defaults to 512

189

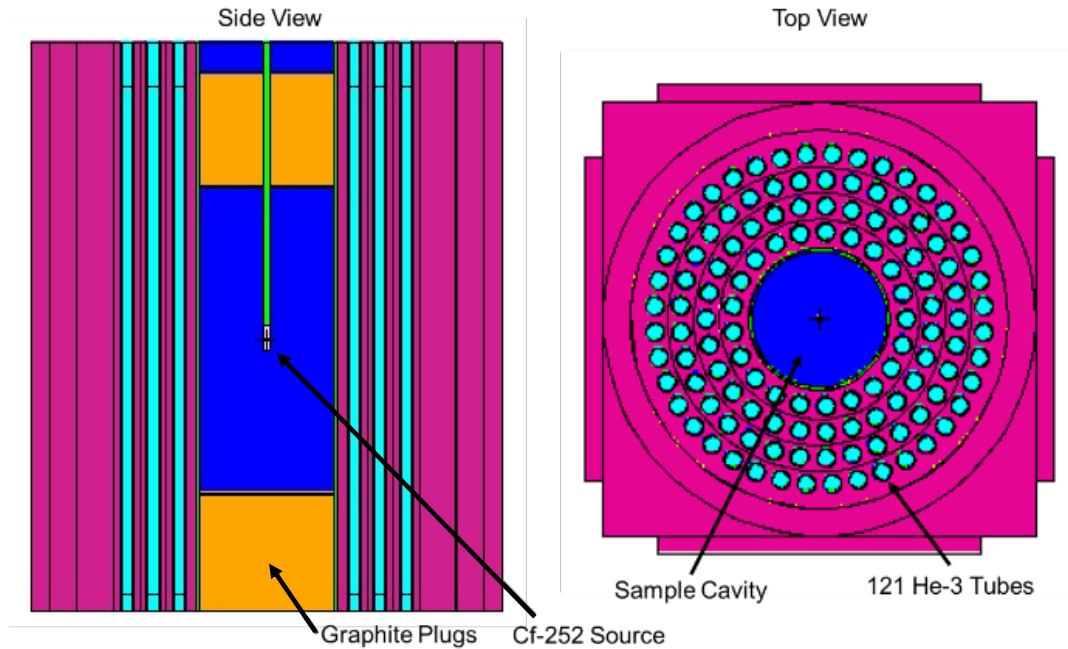
190 A broad overview of the process for defining a gas-filled detector in DRiFT follows. First,  
191 the user must indicate the geometry of their detector. Three geometry options are available in the  
192 code: the most common is a cylindrical tube, though a spherical detector with a point anode and  
193 a spherical detector with a wire anode are also available. Users then must specify their fill and  
194 quench gases, along with their relative compositions. Currently, He-3 and BF<sub>3</sub> are available for  
195 fill gases and CO<sub>2</sub> and CH<sub>4</sub> are available for quench gases. One fill gas and one quench gas can  
196 be mixed at a ratio generally ranging from 100% fill gas to 95% fill gas. The tube's pressure,  
197 temperature, and applied voltage can be specified in the ranges given in Table 1. Details of the  
198 tube's geometry must then be provided. The length and radius of the gas tube (in the case of a  
199 cylinder) or the radius of the tube (in the case of a sphere) must be provided, along with the radius  
200 of the central anode wire (in the case of a point anode, this is the radius of the sphere that  
201 represents the anode). The location and orientation of the detector in space must then be  
202 provided. The location of the base of the detector is first specified. The base of the detector is  
203 defined, in the case of a cylinder, as the flat surface from which the vector representing the  
204 cylinder extends, and in the case of a sphere, as the center point of the sphere. The orientation  
205 of the detector is given as a unit vector, which does not need to be normalized, representing the  
206 central axis of the cylinder extending from the base. Detector orientation is not needed for a  
207 spherical detector. Finally, whether DRiFT should simulate inactive areas at the ends of the gas  
208 tube can be specified; inactive areas are not supported for spherical detector geometries.

209 The preamplifier attached to the gas-filled detector can be customized as well. This affects  
210 several potential electronic artifacts that could be introduced in the gas tube response. First,  
211 pileup can be enabled or disabled, controlling whether multiple pulses that occur close together  
212 temporally can pileup on each other and be counted as one pulse. The pulse shape itself (which  
213 affects the likelihood of pulses to pileup on each other) can also be customized by specifying a  
214 shaping time constant, or by providing a tube capacitance and load resistance so the shaping  
215 time constant can be calculated. Dead time can be enabled and customized, allowing for pulses  
216 within a specified time window of an original pulse to be ignored. This dead time can also be  
217 specified to be paralyzable or non-paralyzable.

218 In addition to the settings described above, several diagnostic capabilities of interest for  
219 gas-filled detectors are also available as part of the DRIFT toolkit. First, events that are from room  
220 return, where radiation interacts in the walls, ceiling, or elsewhere in the environment before  
221 scattering into the detector, can be flagged and output. This capability is demonstrated by an  
222 experiment later in this work. The capability to flag pulse pileup events for separate analysis is  
223 also provided, along with the ability to flag events that are correlated in time or from the same  
224 source particle.

#### 225 Epithermal Neutron Multiplicity Counter Validation

226 An experiment was performed on the Epithermal Neutron Multiplicity Counter (ENMC) [21]  
227 at Los Alamos National Laboratory to demonstrate and validate the gas-filled detector capabilities  
228 provided by DRIFT [22]. A diagram of the ENMC generated using the MCNP code is given in  
229 Figure 3. The ENMC is a well counter designed for neutron multiplicity counting with an intrinsic  
230 efficiency of 63.5% that contains 121 He-3 tubes with an active length of 71.1 cm and a radius of  
231 2.54 cm, filled to 10 atm and operated at a nominal voltage of 1720 V. These He-3 tubes are  
232 connected to 27 AMPTEK A111 amplifiers to read out the signal. The well at the center of the  
233 detector is 19 cm in diameter and has a height of 75 cm. During operation, the well is covered by  
234 a graphite and cadmium plug with a diameter of 18.5 cm and a length of 31.5 cm.



235

236 Figure 3: A diagram of the ENMC detector, containing 121 He-3 tubes centered around a central  
 237 cavity. The Cf-252 source is suspended in place from the top of the detector by a steel rod.

238 Measurements were taken with a 21.6  $\mu\text{Ci}$  (100,000 n/s) Cf-252 neutron source at 24  
 239 vertical positions at the centerline in the detector well using the INCC6 data acquisition software  
 240 [23]. These measurements were taken at evenly spaced intervals between the bottom of the well  
 241 and the top, including traveling into the graphite plug. Measurements were specifically done this  
 242 way to probe the ability of DRiFT to model the effects of the inactive regions of the He-3 detectors,  
 243 which were 6.27 cm in length at the top of the detector tubes and 2.46 cm in length at the bottom.  
 244 Two-minute-long measurements, divided into 6, 20 second cycles, were taken at each position to  
 245 obtain a count rate. This resulted, at its maximum, in a singles rate around 60,000 cps with an  
 246 uncertainty of around 40 cps; the singles rate was used for this experiment instead of doubles or  
 247 other multiplicities for a more straightforward comparison with results from the MCNP code. While  
 248 DRiFT has the capability to model neutron multiplicities and flag them as reals and accidentals,  
 249 this was not utilized in this experiment in order to not confound effects from the inactive end-tube  
 250 regions.

251 After the experiment had concluded, the setup was recreated as an MCNP input deck.  
 252 Simulations were repeated with source definitions to match the experimental conditions previously  
 253 carried out. As with the experimental measurement, the number of counts, given by the number  
 254 of neutron absorptions in the active portion of the He-3 detector, were recorded. Two sets of  
 255 simulations were carried out. In the first, the top 6.27 cm and the bottom 2.46 cm of the He-3  
 256 tubes were treated as inactive regions; that is, they were created as separate MCNP cells and  
 257 interactions that occurred within those regions did not contribute to the overall count rate. In the  
 258 second set of simulations, the ends of the He-3 tubes were treated as active regions so that  
 259 interactions that occurred within them did count as detector events and contributed to the  
 260 detector's count rate.

261 In addition to the information described above, each MCNP simulation also output a  
262 PTRAC file that recorded both the origin of each neutron and the location of neutron absorptions  
263 in the geometry. These PTRAC output files could then be fed into DRIFT.

264 DRIFT was then used to post-process the MCNP simulations to better capture the  
265 response of the gas tubes to the Cf-252 source. Details of the He-3 tubes' geometries were input  
266 into DRIFT, including the tube length and radius, along with the length of the inactive regions on  
267 both sides of the tube. The composition of the gas and its pressure were also input according to  
268 the detector's specifications. Finally, the applied voltage to the tubes and the details of the  
269 AMPTEK A111 charge sensitive preamplifier – such as the detector's dead time and the pre-  
270 amplifier's 190 ns shaping time – were input. DRIFT then read in the MCNP PTRAC files  
271 described in the previous section and simulated the response of the He-3 tubes to the recorded  
272 neutron absorptions. This process was repeated for each measurement point in the well detector.  
273 Because the specifications of the tubes did not change between points, the detector specifications  
274 given in the DRIFT configuration file did not need to be modified between runs, other than to  
275 change the name of the PTRAC file being read. The number of detection events recorded were  
276 then read out by DRIFT.

277 A comparison of the experimental results and both sets of simulation results from the  
278 MCNP code alone and from the MCNP code plus DRIFT are presented in Table 3. It can be seen  
279 from the table that using the MCNP code plus DRIFT produces the results most in agreement with  
280 the experimental results. This is particularly true towards the top of the detector where the inactive  
281 ends of the He-3 tubes have the most effect. Treating the end-tubes as entirely inactive regions,  
282 the third column of the table, underestimates the count rate of the detector in this region. Treating  
283 the end tubes as entirely active regions, the fourth column of the table, also does not match  
284 experimental results and overestimates the count rate between 30 and 35 cm. Most simply, using  
285 the MCNP code in conjunction with DRIFT more accurately reflects the count rate across the  
286 detector than without DRIFT.

287

288

289

290

291

292

293

294

295

296

297 Table 3: The relative difference of different simulated results from experimental results. Points  
 298 between 38 and 65 cm are skipped as both simulation methods simulations are in very good  
 299 agreement with the experimental results.

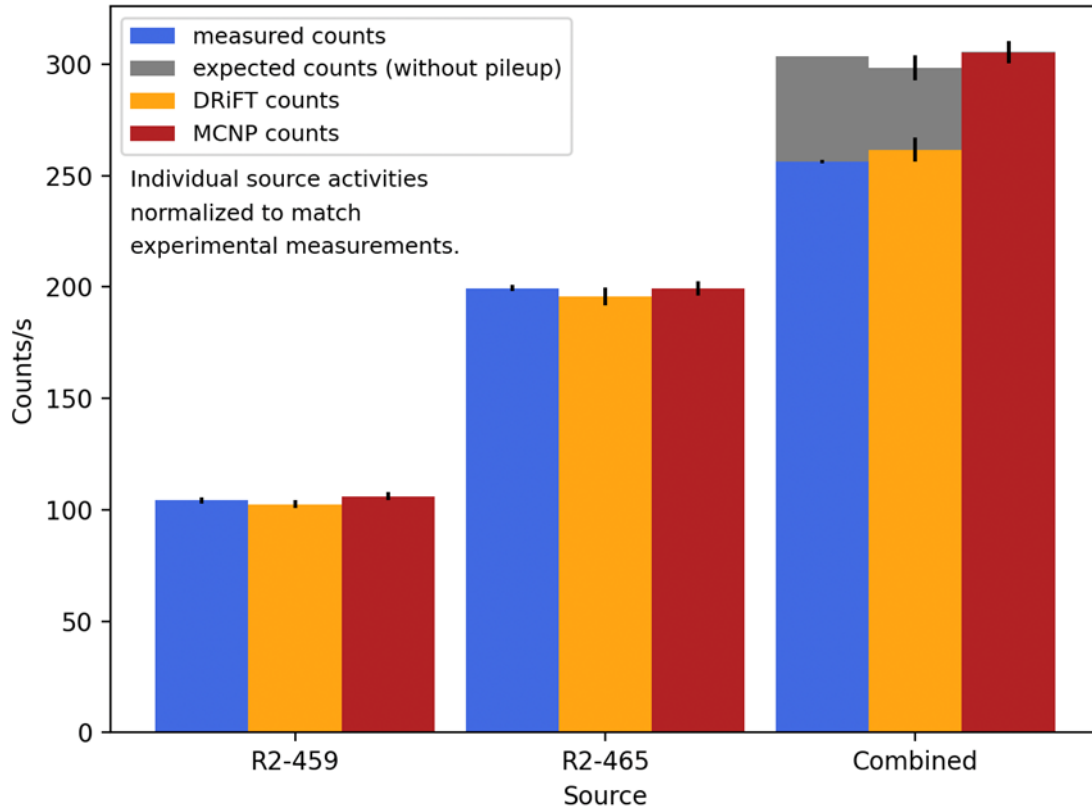
Distance of Source from the Top of the Detector (cm)	Measured Singles Count Rate (cps)	Relative difference from experimental results of...		
		MCNP Code with Inactive Tube Ends	MCNP Code with Active Tube Ends	MCNP Code + DRiFT
<b>21.1</b>	3.26E+04	-63.77%	-35.51%	-14.62%
<b>23.6</b>	4.01E+04	-36.30%	-9.11%	5.46%
<b>26.1</b>	4.66E+04	-21.59%	2.00%	5.24%
<b>27.4</b>	4.95E+04	-10.51%	8.06%	5.32%
<b>28.7</b>	5.22E+04	-4.79%	8.31%	4.50%
<b>30.0</b>	5.45E+04	-0.08%	8.38%	4.13%
<b>31.3</b>	5.67E+04	1.12%	5.91%	2.94%
<b>33.8</b>	5.97E+04	0.11%	2.54%	0.79%
<b>36.4</b>	6.02E+04	-0.24%	1.57%	0.62%
<b>38.9</b>	6.06E+04	0.04%	1.55%	0.68%
...	Skipping positions where all simulations are in good agreement			
<b>65.0</b>	6.17E+04	-0.92%	-1.11%	-0.41%
<b>67.6</b>	6.12E+04	-0.46%	-0.57%	-0.01%
<b>70.2</b>	6.08E+04	-1.15%	-1.17%	-0.13%
<b>72.7</b>	6.03E+04	-0.82%	-0.78%	0.05%
<b>75.2</b>	5.97E+04	-0.10%	0.08%	0.36%

300

301 Pulse Pileup Example

302 DRiFT, as described above, has the capacity to model relevant effects from the  
 303 detector's electronics. Two of such effects are pulse pileup and deadtime. These effects are  
 304 most significant when measuring high-activity sources that result in large count rates, though  
 305 the design of the detector system and preamplifier may influence the significance of each effect  
 306 for lower count rates. Both pileup and dead time can result in the loss of events that occur in  
 307 the detector system.

308 The effects of pulse pileup were measured using a two-tube He-3 detector system  
 309 exposed to different Cf-252 neutron sources. Two sources – a lower activity source (designated  
 310 R2-459), with an activity of 10.4  $\mu\text{Ci}$  ( $\sim 48,000$  n/s), and a higher activity source (designated R2-  
 311 465), with an activity of 20.1  $\mu\text{Ci}$  ( $\sim 93,000$  n/s) – were measured individually to establish a  
 312 baseline tube response. Both sources were then measured together, and the difference  
 313 between the expected count rate (the simple sum of the count rates from the individual tube  
 314 measurements) and the measured count rate was observed. The results of these  
 315 measurements are provided in Figure 4. For this experiment, no distinction was made between  
 316 pulse pileup and deadtime, as both phenomena result in the loss of events in the He-3 tubes.



317  
 318 Figure 4: A comparison of the expected and actual count rate when exposing a He-3 detector  
 319 system to two Cf-252 sources, demonstrating DRiFT's ability to model pulse pileup. The  
 320 measured counts are presented in blue (left bar), with the results from the MCNP code + DRiFT  
 321 presented in orange (center bar), and the results from the MCNP code alone presented in red  
 322 (right bar). Source activities in the MCNP code were normalized to match experimental results  
 323 for individual measurements.

324 It can be seen in Figure 4 that, compared to the expectation based on the results from  
 325 the individual source measurements, the count rate observed for the combined measurement is  
 326 17% lower than expected, with around 250 counts per second measured rather than the 300  
 327 counts per second expected.

328 The experimental setup was recreated in an MCNP geometry and simulated. The  
 329 results of this simulation, which does not consider pulse pileup or deadtime, are also given in  
 330 Figure 4. These results were post-processed using DRiFT to accurately simulate pileup effects.

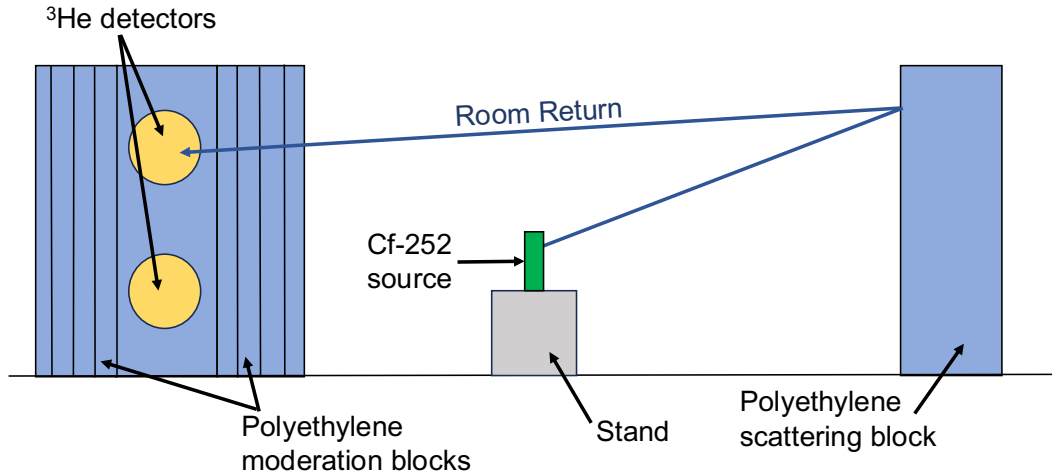
331 The results from the MCNP code plus DRIFT are found to be in good agreement with the  
332 experimental results. The count rate from the combined sources reported by DRIFT was found  
333 to be 17% lower than those reported by the MCNP code alone and are within 2.1% of the  
334 experimental results. These results show that DRIFT is able to accurately represent the effects  
335 of pulse pileup on a detector's count rate in this case. Overall, these experiments have  
336 demonstrated the ability of DRIFT to accurately model the response of gas-filled neutron  
337 detectors in two detector configurations. An additional experiment was also conducted to  
338 demonstrate DRIFT's ability to provide diagnostic information for the results provided by a  
339 detector system.

#### 340 Room Return Example

341 DRIFT can also provide useful diagnostic information to the user alongside its simulation  
342 of a He-3 gas detector response. One such diagnostic capability is to flag room return events,  
343 defined as neutrons that interact in the surrounding environment before scattering into the  
344 detector, as opposed to neutrons that travel directly to the detector after being created. The  
345 prevalence of room return will depend heavily on the geometry of the room around the source  
346 and detector system, and it can be of interest to determine the effect that this surrounding  
347 geometry has on the signal.

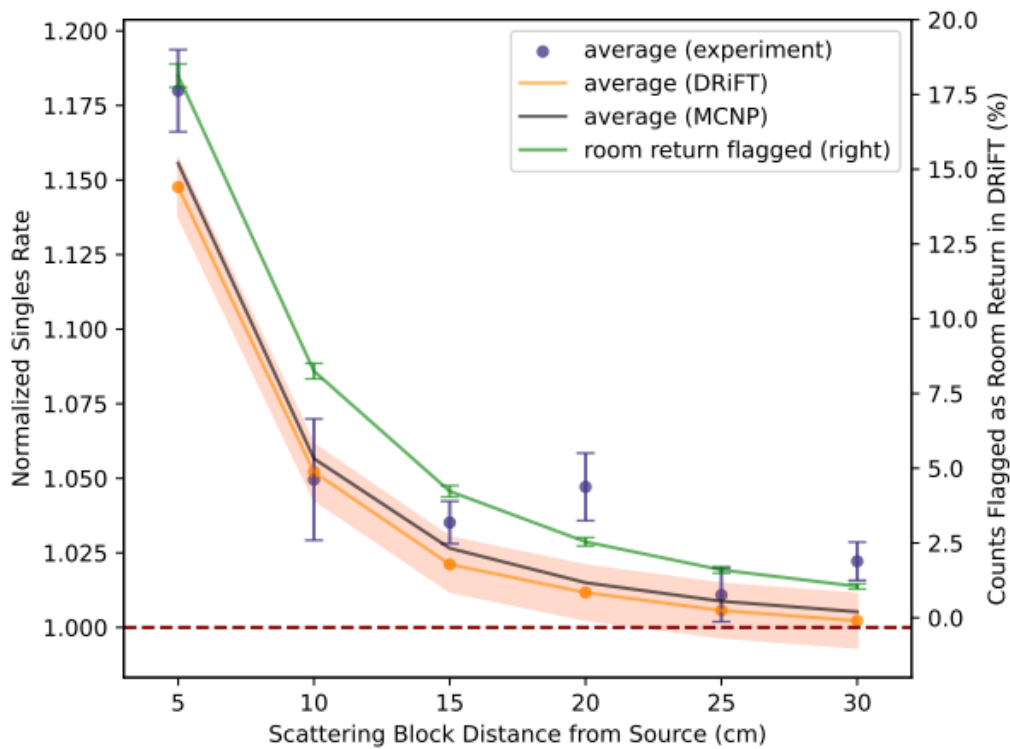
348 During the execution of DRIFT, the user can define any number of MCNP cells that will  
349 be treated as the "room" around the detector system. Any neutron or gamma ray that interacts  
350 in or passes through one of these cells before interacting in the detector is flagged as "room  
351 return". This flag is carried throughout the rest of the analysis and is output alongside the rest of  
352 the information for the detection event. This allows detection events that are from room return  
353 to be kept separate by the user in future analyses; this allows them, for example, to study how a  
354 detector's positioning in a room affects the results of an experiment due to room return off of the  
355 walls and ceiling.

356 To demonstrate DRIFT's ability to flag room return events, an experiment was performed  
357 with a two-tube He-3 detector system, as depicted in Figure 5. A Cf-252 source was placed  
358 between the detector system and a standalone block of polyethylene, referred to below as the  
359 scattering block. Some neutrons emitted from the Cf-252 source travel directly to the detector  
360 system and are recorded; others travel in the opposite direction, backscatter off the scattering  
361 block, and then travel to the detector system and are recorded. The prominence of the  
362 backscatter room return effect depends on the distance between the source and the scattering  
363 block. Varying this distance varies the amount of room return events that occur. The results of  
364 the experiment for scattering block distances between 5 and 30 cm are presented in Figure 6.  
365 All results are for singles events; too few coincident double events were recorded in the detector  
366 system to be used for this analysis.



367

368 Figure 5: A side-view diagram of the room return experiment setup. The distance between the  
 369 source (center) and scattering block (right) is varied to affect the number of room return events  
 370 seen by the detectors (left).



371

372 Figure 6: The variation of the count rate of a two-tube He-3 detector system as a polyethylene  
 373 scattering block is moved closer to the source, on the opposite side as the detector. On the  
 374 secondary axis, the percentage of events tagged as room return events is plotted. All values  
 375 are normalized to a measurement/simulation without a scattering block included (represented by  
 376 the red dashed line).

377 The data shows that, as expected based on intuition, the closer the scattering block was  
 378 brought to the source, the higher the count rate became due to an increased number of room

379 return events. This can be verified using DRIFT's diagnostic capabilities. The experimental  
380 setup was recreated in the MCNP code and post-processed by DRIFT. The overall count rates  
381 generated by DRIFT were equivalent to the experimental results, as seen in Figure 6. Plotted  
382 on the secondary axis is the percentage of events flagged by DRIFT to be room return events.  
383 At the smallest source-scattering block separation, around 17% of the events were attributed to  
384 room return, while at the largest separation, almost none of the events were attributed to room  
385 return. DRIFT thus demonstrates, through its diagnostic capability, that the increase seen at  
386 short separation distances is entirely a result of an increase in the number of room return events  
387 in the detector.

### 388 Conclusions and Future Work

389 The capability to model gas-filled detector and pre-amplifier responses with DRIFT has  
390 been demonstrated and validated. Post-processing MCNP outputs with DRIFT better represents  
391 the behavior of the detector than is possible with the MCNP code alone, as DRIFT can better  
392 model effects from the inactive ends of the detector tubes and effects from downstream  
393 electronics. DRIFT can also provide useful diagnostic information, such as flagging room return  
394 events, for better understanding the simulation scenario. These capabilities are included in the  
395 most recent public release of DRIFT. Future DRIFT development will seek to further refine and  
396 expand these capabilities, as well as expanding the scintillator capabilities and introducing  
397 semiconductor detector capabilities.

### 398 Acknowledgements

399 Funding for this work has been provided by the U.S. Department of Energy at Los Alamos  
400 National Laboratory (operated by Triad National Security, LLC, for the National Nuclear Security  
401 Administration) under Contract No. 89233218CNA000001), Technology Evaluation and  
402 Demonstration Projects.

### References

- [1] R. Runkle, A. Bernstein, P. Vanier, Securing special nuclear material: Recent advances in neutron detection and their role in nonproliferation, J.Appl.Phys. 108(13) (2010) 111101. <https://doi.org/10.1063/1.3503495>
- [2] R. Kouzes, E. Siciliano, J. Ely, P. Keller, R. McCoon, Passive neutron detection for interdiction of nuclear material at borders, Nucl.Instr.Meth.A, 584(2-3) (2008), 383-400. <https://doi.org/10.1016/j.nima.2007.10.026>
- [3] R. Cooper, SNS detector plans, Nucl.Instr.Meth.A, 529(1-3) (2004), 394-398. <https://doi.org/10.1016/j.nima.2004.05.018>
- [4] T. Goorley, M. James, T. Booth, F. Brown, J. Bull, L. Cox, J. Durkee, et al., Initial MCNP6 release overview, Nucl.Technology 180(3) (2012) 298-315. <https://doi.org/10.13182/NT11-135>

- 
- [5] M. Andrews, C. Bates, E. McKigney, A. Mullen, S. Woldegiorgis, M. Rising, M. Marcath, A. Sood, DRIFT - Release 1.0.0 Organic Scintillators, Los Alamos National Laboratory Technical Report (2021). <https://doi.org/10.2172/1821338>
- [6] M. Andrews, A. Mullen, S. Woldegiorgis, M. Rising, A DRIFT Organic Scintillator Executable for Nuclear Safeguards Applications, J.Nucl.Mater.Management, 50(2) (2022) 20-27. <https://www.ingentaconnect.com/openurl?genre=article&eissn=0893-6188&volume=50&issue=2&spage=20&epage=27&aulast=Andrews>
- [7] M. Andrews, C. Bates, E. McKigney, C. Solomon, and A. Sood, Organic scintillator detector response simulations with DRIFT, Nucl.Instr.Meth.A, 830 (2016) 466-472. <https://doi.org/10.1016/j.nima.2016.06.011>
- [8] M. Andrews, A. Mullen, DRIFT Current Mode, Trigger Settings and Flexible Detector Specifications Applied to Scintillator Arrays. Radiat.Phys.Chemistry. Submitted. <http://dx.doi.org/10.2139/ssrn.4509444>
- [9] C. Ahl, M. Andrews, E. Lukosi, An HPGe semiconductor detector response function for use in DRIFT, Los Alamos National Laboratory Technical Report (2022). LA-UR-22-30555
- [10] M. Andrews, A. Mullen, C. Bates, L. Rondini, DRIFT – Release 2.1.1: Organic Scintillators and Gas Detectors, Los Alamos National Laboratory Technical Report (2023). LA-UR-23-29836
- [11] J. Als-Nielsen, O. Dietrich, Slow Neutron Cross Sections for He-3, B, and Au, Phys.Rev. 133(4B) (1964), B925--B929. <https://doi.org/10.1103/PhysRev.133.B925>
- [12] G. Whan, Procedures for PuO<sub>2</sub> Field Measurements with an HLNC-II, Los Alamos National Laboratory Technical Report (1987). <https://inis.iaea.org/search/19002798>
- [13] P. Peplowski, Z. Yokley, M. Liebel, S. Cheng, R. Elphic, S. Hoogerheide, D. Lawrence, J. Nico, Position-dependent Neutron Detection Efficiency Loss in <sup>3</sup>He Gas Proportional Counters, Nucl.Instr.Meth.A 982 (2020) 164574. <https://doi.org/10.1016/j.nima.2020.164574>
- [14] D. Pfeiffer, L. De Keukeleere, C. Azevedo, F. Belloni, S. Biagi, V. Grichine, L. Hayen, A. Hanu, I. Hřivnáčová, V. Ivanchenko, V. Krylov, H. Schindler, R. Veenhof, Interfacing Geant4, Garfield++ and Degrad for the simulation of gaseous detectors, Nucl.Instr.Meth.A, 935 (2019) 121-134. <https://doi.org/10.1016/j.nima.2019.04.110>.
- [15] B. van der Ende, E. Rand, A. Erlandson, L. Li, Use of SRIM and Garfield with Geant4 for the characterization of a hybrid 10B/<sup>3</sup>He neutron detector, Nucl.Inst.Meth.A, 894 (2018) 138-144. <https://doi.org/10.1016/j.nima.2018.03.056>
- [16] L. Rolandi, W. Riegler, W. Blum, Particle Detection with Drift Chambers, Springer-Verlag, Berlin, 2008, p.157-180.

- 
- [17] J. Ziegler, J. Biersack, U. Littmark, The Stopping and Range of Ions in Matter, Pergamon Press (1985). <http://www.srim.org/>
- [18] S. F. Biagi, Monte Carlo simulation of electron drift and diffusion in counting gases under the influence of electric and magnetic fields, Nucl.Instr.Meth.A 421 (1999), 234. [https://doi.org/10.1016/S0168-9002\(98\)01233-9](https://doi.org/10.1016/S0168-9002(98)01233-9)
- [19] H. Schindler, R. Veenhof, Garfield++, <https://garfieldpp.web.cern.ch> (accessed on November 13th, 2023).
- [20] D. Wilkinson, Ionization chambers and counters, Cambridge University Press, New York, 1950.
- [21] H. Menlove, C. Rael, K. Kroncke, K. DeAgüero, Manual for the Epithermal Neutron Multiplicity Detector (ENMC) for Measurement of Impure MOX and Plutonium Samples, Los Alamos National Laboratory Technical Report (2004). <https://inis.iaea.org/search/48014746>
- [22] A. Mullen, M. Andrews, C. Thompson, Simulation of He-3 Neutron Detectors with DRiFT, a Detector Response Function Toolkit, abstract in: 2023 IEEE Nuclear Science Symposium and Medical Imaging Conference, Vancouver, BC, Canada, 2023.
- [23] H. Nordquist, and M. Swinhoe, INCC 6.0 - LANL's latest neutron coincidence counting software, Los Alamos National Laboratory Technical Report (2017). <https://www.osti.gov/biblio/1407860>